

SUSY-QCD Corrections to $W^\pm H^\mp$ Associated Production at the CERN Large Hadron Collider

Jun Zhao, Chong Sheng Li*, and Qiang Li

Department of Physics, Peking University, Beijing 100871, China

Abstract

We calculate the SUSY-QCD corrections to the inclusive total cross sections of the associated production processes $pp \rightarrow W^\pm H^\mp + X$ in the Minimal Supersymmetric Standard Model(MSSM) at the CERN Large Hadron Collider(LHC). The SUSY-QCD corrections can increase and decrease the total cross sections depending on the choice of the SUSY parameters. When $\mu < 0$ the SUSY-QCD corrections increase the leading-order (LO) total cross sections significantly for large $\tan\beta$ (~ 40), which can exceed 10% and have the opposite sign with respect to the QCD and the SUSY-EW corrections, and thus cancel with them to some extent. Moreover, we also investigate the effects of the SUSY-QCD on the differential distribution of cross sections in transverse momentum p_T and rapidity Y of W-boson, and the invariant mass $M_{W^+H^-}$.

PACS numbers: 12.38.Bx, 12.60.Jv, 14.70.Fm, 14.80.Cp

* Electronics address: csli@pku.edu.cn

A. Introduction

The Higgs mechanism[1] plays a key role for spontaneous breaking of the electroweak symmetry both in the standard model(SM)and in the minimal supersymmetric extension of the SM(MSSM)[2]. The SM contains one neutral CP-even Higgs boson, while the MSSM accommodates five physical Higgs bosons: the neutral CP-even h^0 and H^0 bosons, the neutral CP-odd A^0 boson, and the charged H^\pm boson pair. The charged Higgs bosons do not belong to the spectrum of the SM, so the discovery of them would be an unambiguous sign of new physics beyond the SM. Therefore, the search of charged Higgs bosons become one of the prime tasks in future high-energy experiments, especially at the LHC[3]. At hadron colliders, the charged Higgs bosons H^\pm could appear as the decay product of primarily produced top quarks if the mass of H^\pm is smaller than the $m_t - m_b$. For heavier H^\pm , the main channels for single charged Higgs production may be those associated with heavy quark, such as $gb \rightarrow H^- t$ [4] and $qb \rightarrow q' b H^-$ [5]. Although these processes give rather large production rates, they suffer from also large QCD backgrounds, especially when the H^\pm mass is above the threshold of $t\bar{b}$. And the channels for pair production are $q\bar{q}$ annihilation and the loop-induced gg fusion processes [6], which is also severely plagued by the QCD backgrounds.

Another attractive mechanism of H^\pm production in association with W^\mp bosons at hadron colliders has been proposed and analyzed in the Ref. [7], which found that the $W^\mp H^\pm$ production would have a sizeable cross section and its signal should have a significant rate at the LHC unless m_{H^\pm} is very large. The dominant partonic subprocesses of $W^\mp H^\pm$ associated production are $b\bar{b} \rightarrow W^\mp H^\pm$ at the tree-level and $gg \rightarrow W^\mp H^\pm$ at the one-loop level. In these processes, the leptonic decays of W-boson would serve as a spectacular trigger for the H^\pm search. A careful signal-versus-background analysis has been done in Refs.[8]. The detailed computation of the cross section of the gg fusion process can be found in the Ref. [9]. For the $b\bar{b}$ annihilation process, the $\mathcal{O}(\alpha_{ew} m_{t(b)}^2/m_W^2)$ and $\mathcal{O}(\alpha_{ew} m_{t(b)}^4/m_W^4)$ SUSY-EW and the $\mathcal{O}(\alpha_s)$ QCD corrections also have been calculated in Refs. [10] and [11], respectively. However, the one-loop SUSY-QCD corrections have not been reported in literatures so far. So in this paper, we present the calculations of the one-loop SUSY-QCD corrections to the process.

This paper is organized as follows. In Section B, we present some analytic results for the

cross sections of $b\bar{b} \rightarrow W^+H^-$. In Section C, we give the numerical predictions for inclusive and differential cross sections at the LHC. The relevant SUSY Lagrangians and the lengthy analytic expressions are summarized in the Appendices.

B. Analytical Results

We consider the associated production of W^+H^- from the collision of the two protons with momentum P_1 and P_2 at the LHC. First, we define the Mandelstam variables of the subprocess $b(p_1)\bar{b}(p_2) \rightarrow W^+(p_3)H^-(p_4)$ as

$$\begin{aligned} s &= (p_1 + p_2)^2 = (p_3 + p_4)^2, \\ t &= (p_1 - p_3)^2 = (p_2 - p_4)^2, \\ u &= (p_1 - p_4)^2 = (p_2 - p_3)^2. \end{aligned} \tag{1}$$

Here the Mandelstam invariants are related by $s + t + u = m_W^2 + m_H^2$.

We carry out the calculations in the t'Hooft-Feynman gauge and use dimensional reduction, which preserves supersymmetry, to regularize the UV divergences in the virtual loop corrections. In order to remove the UV divergences, we renormalize the quark masses in the Yukawa couplings and their wave functions by using the on-mass-shell scheme[12]. Denoting m_{q0} and ψ_{q0} as the bare quark mass and the bare wave function, respectively, the relevant renormalization constants δm_q , δZ_L^q and δZ_R^q are then defined as

$$m_{q0} = m_q + \delta m_q, \tag{2}$$

$$\psi_{q0} = (1 + \delta Z_L^q)^{\frac{1}{2}} \psi_{qL} + (1 + \delta Z_R^q)^{\frac{1}{2}} \psi_{qR}. \tag{3}$$

After calculating the self-energy diagram in Fig. 1, we obtain the explicit expressions of all the renormalization constants as follows:

$$\delta m_q = -\frac{\alpha_s}{3\pi} [m_q [B_1(m_q^2, m_{\tilde{g}}^2, m_{\tilde{q}_1}^2) + B_1(m_q^2, m_{\tilde{g}}^2, m_{\tilde{q}_2}^2)] + m_{\tilde{g}} \sin 2\theta_{\tilde{q}} [B_0(m_q^2, m_{\tilde{g}}^2, m_{\tilde{q}_1}^2) - B_0(m_q^2, m_{\tilde{g}}^2, m_{\tilde{q}_2}^2)]], \tag{4}$$

$$\delta Z_L^q = \frac{2\alpha_s}{3\pi} [\cos^2 \theta_{\tilde{q}} B_1^1 + \sin^2 \theta_{\tilde{q}} B_1^2 + m_q^2 [\dot{B}_1^1 + \dot{B}_1^2 + \frac{m_{\tilde{g}}}{m_q} \sin 2\theta_{\tilde{q}} (\dot{B}_0^1 - \dot{B}_0^2)]], \tag{5}$$

$$\delta Z_R^q = \frac{2\alpha_s}{3\pi} [\sin^2 \theta_{\tilde{q}} B_1^1 + \cos^2 \theta_{\tilde{q}} B_1^2 + m_q^2 [\dot{B}_1^1 + \dot{B}_1^2 + \frac{m_{\tilde{g}}}{m_q} \sin 2\theta_{\tilde{q}} (\dot{B}_0^1 - \dot{B}_0^2)]], \tag{6}$$

where $B_m^i = B_m(m_q^2, m_{\tilde{g}}^2, m_{\tilde{q}_i}^2)$, $\dot{B}_m^i = \dot{B}_m(m_q^2, m_{\tilde{g}}^2, m_{\tilde{q}_i}^2)$ with $q = b, t$ are the two-point integrals [13], $m_{\tilde{q}_i}$ are the squark masses, $m_{\tilde{g}}$ is the gluino mass, and $\theta_{\tilde{q}}$ is the mixing angle of the squarks.

The Feynman diagrams for the subprocess $b\bar{b} \rightarrow H^- W^+$, which include the SUSY-QCD corrections to the process, are shown in Fig.1 and its renormalized amplitude can be written as

$$M^{ren.} = M^0 + M^{vir.} + \delta M^{count.}. \quad (7)$$

Here M^0 is the tree-level amplitude, which is given by summing over the s- and t-channel amplitudes:

$$M^0 = M^{s0} + M^{t0}, \quad (8)$$

with

$$M^{s0} = \frac{2\pi\alpha m_b}{m_w \sin^2 \theta_w} \left[S_b(A_4 + A_3) + P_b(A_4 - A_3) \right], \quad (9)$$

$$M^{t0} = \frac{2\pi\alpha}{m_w \sin^2 \theta_w} \frac{1}{t - m_t^2} \left[m_t^2 \cot \beta A_{10} + m_b \tan \beta (A_{11} - 2A_3) \right], \quad (10)$$

where S_b and P_b are defined by

$$S_b = \frac{1}{\cos \beta} \left[-\frac{\sin \alpha \cos(\alpha - \beta)}{s - m_{h^0}^2} + \frac{\cos \alpha \sin(\alpha - \beta)}{s - m_{H^0}^2} \right], \quad (11)$$

$$P_b = \frac{1}{\cos \beta} \frac{\sin \beta}{s - m_{A^0}^2}, \quad (12)$$

A_i are reduced standard matrix elements, which are given by

$$\begin{aligned} A_1 &= \bar{v}(p_2) P_R u(p_1) p_1 \cdot \varepsilon(p_4), \\ A_2 &= \bar{v}(p_2) P_L u(p_1) p_1 \cdot \varepsilon(p_4), \\ A_3 &= \bar{v}(p_2) P_R u(p_1) p_3 \cdot \varepsilon(p_4), \\ A_4 &= \bar{v}(p_2) P_L u(p_1) p_3 \cdot \varepsilon(p_4), \\ A_5 &= \bar{v}(p_2) \not{p}_3 P_R u(p_1) p_1 \cdot \varepsilon(p_4), \\ A_6 &= \bar{v}(p_2) \not{p}_3 P_L u(p_1) p_1 \cdot \varepsilon(p_4), \\ A_7 &= \bar{v}(p_2) \not{p}_3 P_R u(p_1) p_3 \cdot \varepsilon(p_4), \end{aligned} \quad (13)$$

$$A_8 = \bar{v}(p_2) \not{p}_3 P_L u(p_1) p_3 \cdot \varepsilon(p_4),$$

$$A_9 = \bar{v}(p_2) \not{\varepsilon}(p_4) P_R u(p_1),$$

$$A_{10} = \bar{v}(p_2) \not{\varepsilon}(p_4) P_L u(p_1),$$

$$A_{11} = \bar{v}(p_2) \not{p}_3 \not{\varepsilon}(p_4) P_R u(p_1),$$

$$A_{12} = \bar{v}(p_2) \not{p}_3 \not{\varepsilon}(p_4) P_L u(p_1),$$

and $M^{vir.}$ contains the radiative corrections from the one-loop self-energy, vertex, and box diagrams, of which corresponding amplitudes are shown in Appendix B. The counter-term $\delta M^{count.}$ contains the contributions from the corresponding vertex and self-energy counterterms, which are given by

$$\delta M^{vs} = M^{s0} \left(\frac{\delta m_b}{m_b} + \frac{1}{2} \delta Z_R^b + \frac{1}{2} \delta Z_L^b \right), \quad (14)$$

$$\begin{aligned} \delta M^{vt1} = & \frac{2\pi\alpha}{m_w \sin^2 \theta_w} \frac{1}{t - m_t^2} \left[m_t^2 \cot \beta \left(\frac{\delta m_t}{m_t} + \frac{1}{2} \delta Z_R^t + \frac{1}{2} \delta Z_L^b \right) A_{10} \right. \\ & \left. + m_b \tan \beta \left(\frac{\delta m_b}{m_b} + \frac{1}{2} \delta Z_L^t + \frac{1}{2} \delta Z_R^b \right) (A_{11} - 2A_3) \right], \end{aligned} \quad (15)$$

$$\delta M^{vt2} = M^{t0} \left(\frac{1}{2} \delta Z_L^b + \frac{1}{2} \delta Z_L^t \right), \quad (16)$$

$$\begin{aligned} \delta M^{self} = & \frac{2\pi\alpha}{m_w \sin^2 \theta_w} \frac{1}{t - m_t^2} \left[m_t^2 \cot \beta \left(\frac{\delta m_t}{m_t} + \frac{1}{2} \delta Z_L^t + \frac{1}{2} \delta Z_R^t \right) A_{10} \right. \\ & \left. + m_b \tan \beta \left(\delta Z_L^t + \frac{2m_t^2}{t - m_t^2} \frac{\delta m_t}{m_t} \right) (A_{11} - 2A_3) \right]. \end{aligned} \quad (17)$$

The partonic cross section can be written as following:

$$\hat{\sigma} = \int_{-1}^1 dz \frac{1}{32\pi s^2} \lambda^{1/2} \overline{|M^{ren.}|^2} = \int_{t_-}^{t_+} dt \frac{1}{16\pi s^2} \overline{|M^{ren.}|^2}, \quad (18)$$

where $\lambda \equiv (s + m_W^2 - m_{H^-}^2)^2 - 4sm_W^2$, $t_{\pm} = \frac{1}{2}[m_{H^-}^2 + m_W^2 - s \pm \lambda^{1/2}]$, and $\overline{|M^{ren.}|^2}$ is the renormalized amplitude squared, which is given by

$$\overline{|M^{ren.}|^2} = \overline{\sum} |M^0|^2 + 2\text{Re} \overline{\sum} M^0 [M^{vir.} + \delta M^{count.}]^\dagger, \quad (19)$$

where the colors and spins of the outgoing particles have been summed over, and the colors and spins of incoming ones have been averaged over. We notice that the color average factors of LO and NLO amplitudes squared are different: $\frac{1}{3} \times \frac{1}{3} \text{Tr} \mathbb{1} = \frac{1}{3}$ for LO amplitudes, and $\frac{1}{3} \times \frac{1}{3} \text{Tr}(\mathbf{T}^a \mathbf{T}^a) = \frac{4}{9}$ for NLO ones. The both spin average factors are the same $\frac{1}{2} \times \frac{1}{2} = \frac{1}{4}$.

The total cross section at the LHC is obtained by convoluting the partonic cross section with the parton distribution functions (PDFs) $G_{b,\bar{b}/p}$ in the proton:

$$\sigma = \int_{\tau_0}^1 dx_1 \int_{\tau_0/x_1}^1 dx_2 [G_{b/p}(x_1, \mu_f) G_{\bar{b}/p}(x_2, \mu_f) + (x_1 \leftrightarrow x_2)] \hat{\sigma}(\tau S), \quad (20)$$

where μ_f is the factorization scale and $S = (P_1 + P_2)^2$, P_1 and P_2 are the four-momentum of the incident hadrons, $\tau_0 = \frac{(m_W + m_{H^-})^2}{S}$, $\tau = x_1 x_2$, and x_1 and x_2 are the longitudinal momentum fractions of initial partons in the hadrons.

In the following, we present the differential cross sections in the transverse momentum p_T and rapidity Y of the W-boson, and the invariant mass $M_{W^+H^-}$, respectively. In the center-of-mass frame of initial hadrons, $P_1 = \sqrt{S}/2(1, 0, 0, 1)$ and $P_2 = \sqrt{S}/2(1, 0, 0, -1)$, and the four-momentum of W-boson is defined by $p_4 = (E, \mathbf{p}_T, p_L)$. The transverse momentum p_T and the rapidity Y of W-boson, and the invariant mass $M_{W^+H^-}$ are defined by

$$p_T^2 = (E - p_L)(E + p_L) - m_W^2 = \frac{(m_W^2 - t)(m_W^2 - u)}{s} - m_W^2, \quad (21)$$

$$Y = \frac{1}{2} \log \left(\frac{E + p_L}{E - p_L} \right), \quad (22)$$

and

$$M_{W^+H^-}^2 = (p_3 + p_4)^2 = (p_1 + p_2)^2 = s = x_1 x_2 S, \quad (23)$$

respectively.

The three differential cross sections are thus given by

$$\frac{d\sigma}{dp_T} = \int_{\tau_0}^1 dx_1 \int_{\tau_0/x_1}^1 dx_2 [G_{b/p}(x_1, \mu_f) G_{\bar{b}/p}(x_2, \mu_f) + (x_1 \leftrightarrow x_2)] \frac{d\hat{\sigma}}{dp_T}, \quad (24)$$

$$\frac{d\sigma}{dY} = \int_{\tau_0}^1 dx_1 \int_{\tau_0/x_1}^1 dx_2 [G_{b/p}(x_1, \mu_f) G_{\bar{b}/p}(x_2, \mu_f) + (x_1 \leftrightarrow x_2)] \frac{d\hat{\sigma}}{dY}, \quad (25)$$

and

$$\frac{d\sigma}{dM_{W^+H^-}} = \int_{\tau_0}^1 \frac{dx_1}{x_1} \frac{2M_{W^+H^-}}{\tau S} [G_{b/p}(x_1, \mu_f) G_{\bar{b}/p}(x_2, \mu_f) + (x_1 \leftrightarrow x_2)] d\hat{\sigma}, \quad (26)$$

respectively,

with

$$\frac{d\hat{\sigma}}{dp_T} = \frac{1}{32\pi s^2} \lambda^{1/2} \left| \frac{4sp_T}{z\lambda} \right| \overline{|M^{ren.}|^2}, \quad (27)$$

and

$$\frac{d\hat{\sigma}}{dY} = \frac{1}{16\pi s^2} |(s + m_W^2 - m_{H^-}^2) \frac{2u}{(u+1)^2}| \overline{|M^{ren.}|^2}, \quad (28)$$

where $z = \pm \sqrt{1 - \frac{4sp_T^2}{\lambda}}$ and $u = \frac{x_1}{x_2} e^{-2Y}$.

C. Numerical Results and Conclusions

In this section, we present the numerical results for the SUSY-QCD corrections to W^+H^- associated production at the LHC. In our numerical calculations, we used the following set of the SM parameters[14]:

$$\begin{aligned} \alpha_{ew}(m_W) &= 1/128, \quad m_W = 80.419 \text{ GeV}, \quad m_Z = 91.1882 \text{ GeV}, \\ m_b &= 4.25 \text{ GeV}, \quad m_t = 178 \text{ GeV}, \quad \alpha_s(M_Z) = 0.118. \end{aligned} \quad (29)$$

The running QCD coupling $\alpha_s(Q)$ is evaluated at the two-loop order [15], and the CTEQ6M PDFs [16] are used throughout this paper either at the LO or NLO. For simplicity, we neglect the b-quark mass but keep it in the couplings. Moreover, in order to improve the perturbative calculations, we took the running mass $m_b(Q)$ and $m_t(Q)$ evaluated the NLO formula[17]:

$$m_b(Q) = U_6(Q, m_t) U_5(m_t, m_b) m_b(m_b), \quad (30)$$

$$m_t(Q) = U_6(Q, m_t) m_t(m_t), \quad (31)$$

where the evolution factor U_f is

$$\begin{aligned} U_f(Q_2, Q_1) &= \left(\frac{\alpha_s(Q_2)}{\alpha_s(Q_1)} \right)^{d^{(f)}} \left[1 + \frac{\alpha_s(Q_1) - \alpha_s(Q_2)}{4\pi} J^{(f)} \right], \\ d^{(f)} &= \frac{12}{33 - 2f}, \quad J^{(f)} = -\frac{8982 - 504f + 40f^2}{3(33 - 2f)^2}, \end{aligned} \quad (32)$$

and f is the number of the active light quarks.

In addition, to also improve the perturbation calculations, we made the following SUSY replacements in the tree-level couplings[17, 18]

$$m_q(Q) \rightarrow \frac{m_q(Q)}{1 + \Delta m_q} \quad (q = b, t), \quad (33)$$

$$\Delta m_b = \frac{2\alpha_s}{3\pi} M_{\tilde{g}} \mu \tan \beta I(m_{\tilde{b}_1}, m_{\tilde{b}_2}, M_{\tilde{g}}), \quad (34)$$

$$\begin{aligned} \Delta m_t = & -\frac{\alpha_s}{3\pi} \{ \bar{B}_1(0, m_{\tilde{g}}^2, m_{\tilde{t}_1}^2) + \bar{B}_1(0, m_{\tilde{g}}^2, m_{\tilde{t}_2}^2) \\ & - \sin 2\theta_t \left(\frac{m_{\tilde{g}}}{m_t} \right) [\bar{B}_0(0, m_{\tilde{g}}^2, m_{\tilde{t}_1}^2) - \bar{B}_0(0, m_{\tilde{g}}^2, m_{\tilde{t}_2}^2)] \}, \end{aligned} \quad (35)$$

where

$$I(a, b, c) = \frac{1}{(a^2 - b^2)(b^2 - c^2)(a^2 - c^2)} (a^2 b^2 \log \frac{a^2}{b^2} + b^2 c^2 \log \frac{b^2}{c^2} + c^2 a^2 \log \frac{c^2}{a^2}), \quad (36)$$

$$\bar{B}_1 = B_1 + \Delta/2, \bar{B}_0 = B_0 - \Delta \quad (\Delta = 1/\epsilon - \gamma + \ln 4\pi).$$

It is necessary to avoid double counting by subtracting these SUSY-QCD corrections from the renormalization constant. As for the renormalization and factorization scales, we always chose $\mu_r = \mu_f = (m_W + m_{H^-})/2$.

The values of the MSSM parameters taken in our numerical calculations were constrained within the minimal supergravity scenario (mSUGRA)[19], in which there are only five free input parameters at the grand unification where $m_{1/2}$, m_0 , A_0 , $\tan\beta$ and the sign of μ , where $m_{1/2}$, m_0 , A_0 are, respectively, the universal gaugino mass, scalar mass, and the trilinear soft breaking parameter in the superpotential. Given these parameters, all the MSSM parameters at the weak scale are determined in the mSUGRA scenario by using the the program package SUSPECT 2.3[20].

Figs. 2 and 3 show the total cross sections and the relative corrections as functions of $m_{1/2}$ (or $m_{\tilde{g}}$) for $\mu < 0$ and $\tan\beta=4, 10$, and 40 , respectively. The total cross sections decrease with the increasing of $m_{1/2}$ as expected. For small $\tan\beta$, the relative SUSY-QCD corrections are small and can be negligible. For large $\tan\beta$ (~ 40), the relative SUSY-QCD corrections become large and increase when $m_{\tilde{g}}$ increases. Indeed, in our numerical calculations, the dependence of the total cross sections on $m_{\tilde{g}}$ is got through varying $m_{1/2}$. And when $m_{1/2}$ increases, both $m_{\tilde{g}}$ and m_{H^\pm} increase. The increase of m_{H^\pm} decreases the phase spaces of the LO total cross sections, and the magnitudes of the SUSY-QCD corrections also become smaller with the increasing of both $m_{\tilde{g}}$ and m_{H^\pm} . But the decrease rate of the LO total cross sections is larger than the one of the SUSY-QCD corrections, so the relative corrections increase with the increasing of $m_{1/2}$ as shown in Fig. 3.

In Figs. 4 and 5 we present the LO and the SUSY-QCD corrected total cross sections, and the SUSY-QCD corrections as functions of m_{H^-} for $\mu < 0$ and $\tan\beta = 4, 10, 40$, respectively. Both the LO and the SUSY-QCD corrected cross sections decrease when m_{H^-} increases, and

| m_{H^+} GeV | $\tan\beta=4$ | $\tan\beta=10$ | $\tan\beta=40$ |
|---------------|---------------|----------------|----------------|
| 150 | — | — | $\sim 10\%$ |
| 300 | $\sim 0.2\%$ | $\sim -0.2\%$ | $\sim 5\%$ |
| 500 | $\sim 0.8\%$ | $\sim -0.7\%$ | $\sim 4\%$ |

TABLE I: The SUSY-QCD corrections for $\tan\beta=4, 10, 40$ and $m_{H^-} = 150, 300, 500$ GeV, respectively, assuming $A_0 = 250$ GeV, $m_{1/2} = 180$ GeV, $\mu < 0$.

for large $\tan\beta$, the corrections in general enhance the total cross sections for $\mu < 0$. For large $\tan\beta(\sim 40)$ the total cross sections become significant and can reach several tens fb, and even one hundred fb when $m_{H^-} < 200$ GeV, while for small $\tan\beta$ the total cross sections are about several fb and can be neglected. For $\tan\beta = 40$, in general, the corrections can exceed 4%, and even they can reach 10% when $m_{H^-} \sim 150$ GeV. For $\tan\beta = 4, 10$, the magnitude of the corrections are always smaller than 2%. Note that for $\mu < 0$ and $\tan\beta = 4, 10$, the mass of the charged Higgs can not be smaller than about 250 GeV, just as shown by the curves in these figures.

Figs. 6 and 7 show the cross sections and the relative corrections as functions of $\tan\beta$, assuming $m_0 = 160, 400$ GeV, and the sign of $\mu = \pm 1$, respectively. From these figures, we find that the total cross sections for the case of $\mu > 0$ are obviously smaller than those for $\mu < 0$, and that when $\tan\beta$ becomes larger the SUSY-QCD corrections increase the total cross sections for $\mu < 0$, while decrease for $\mu > 0$. For small $\tan\beta$, the variations of these curves are not monotonic because the contributions from the Yukawa coupling $H^- t\bar{b}$ contain not only the terms proportional to $\tan\beta$ but also the ones to $\cot\beta$.

Above results for representative values of m_{H^-} and $\tan\beta$ can be summarized in table I.

In Figs.8-10, we display the differential cross sections as functions of the transverse momentum p_T , the rapidity Y of the W-boson, and the invariant mass $M_{W^+H^-}$, which are given by Eqs.24, 25, and 26, respectively. We find that the SUSY-QCD corrections increase the LO differential cross sections for $\mu < 0$, and decrease ones for $\mu > 0$. The differential cross sections can reach the maximum value at $p_T = 55$ GeV and 70 GeV, $M_{W^+H^-} = 310$ and 370 GeV for $\mu < 0$ and $\mu > 0$, respectively. The differential cross sections in the rapidity of W-boson is symmetric about the axis of $Y=0$ as expected.

Finally, we compare the SUSY-QCD corrections with the $\mathcal{O}(\alpha_{ew}m_{t(b)}^2/m_W^2)$ and

| $\tan\beta$ | $\mathcal{O}(\alpha_{ew}m_{t(b)}^2/m_W^2)$ and $\mathcal{O}(\alpha_{ew}m_{t(b)}^4/m_W^4)$ SUSY-EW corrections [10] | $\mathcal{O}(\alpha_s)$ QCD corrections [11] | SUSY-QCD corrections |
|-------------|---|---|-------------------------|
| 4 | $\sim -14\%$ | $\sim -32\%$ | ~ 0 |
| 40 | $\sim -1\%$ | $\sim -17\%$ | $\sim 8\%$ |

TABLE II: Comparison of the SUSY-QCD corrections with the QCD and SUSY-EW ones, for $\tan\beta = 4, 40$, respectively, assuming $m_{H^-} = 200\text{GeV}$ and $\mu < 0$.

$\mathcal{O}(\alpha_{ew}m_{t(b)}^4/m_W^4)$ SUSY-EW and the $\mathcal{O}(\alpha_s)$ QCD corrections. We notice that the QCD and the SUSY-EW corrections are large and dominate over the SUSY-QCD ones for small $\tan\beta$. When $\tan\beta$ becomes large the SUSY-QCD corrections increase. Although the magnitudes of the SUSY-QCD corrections are still smaller than the ones of the $\mathcal{O}(\alpha_s)$ QCD corrections, they can exceed 10%, which are larger than those of the SUSY-EW corrections. Especially, for $\mu < 0$, the sign of SUSY-QCD corrections is opposite to the ones of the other two corrections, thus the SUSY-QCD corrections can cancel with the SUSY-EW and QCD corrections to some extent. In order to compare these corrections clearly, we show the three corrections to the process $b\bar{b} \rightarrow W^- H^+$ in some typical parameter space in the table II.

In conclusion, we have calculated the SUSY-QCD corrections to the total cross sections for the $W^+ H^-$ associated production in the MSSM at the LHC. The SUSY-QCD corrections can increase and decrease the total cross sections depending on the choice of the SUSY parameters. For $\mu < 0$, the SUSY-QCD corrections can increase the total cross sections significantly, especially for large $\tan\beta$, which have the opposite sign with respect to the QCD and the SUSY-EW corrections, and cancel with them to some extent.

I. ACKNOWLEDGEMENTS

This work was supported in part by the National Natural Science Foundation of China, under grant Nos.10421003 and 10575001, and the Key Grant Project of Chinese Ministry of Education, under grant NO.305001.

Appendix A

In this Appendix, we will list the relevant pieces of SUSY Lagranian. The Yukawa couplings of Higgs and quarks are given by

$$\begin{aligned}\mathcal{L}_{(h^0, H^0, A^0)\bar{b}b} &= \frac{gm_b}{2m_w \cos \beta} \sin \alpha h^0 \bar{b}b - \frac{gm_b}{2m_w \cos \beta} \cos \alpha H^0 \bar{b}b + i \frac{gm_b}{2m_w} \tan \beta A^0 \bar{b} \gamma_5 b, \\ \mathcal{L}_{H^- \bar{t}b} &= \frac{g}{\sqrt{2}m_w} H^+ \bar{t} (m_t \cot \beta P_L + m_b \tan \beta P_R) b + h.c.,\end{aligned}$$

where $P_{L,R} = (1 \mp \gamma_5)/2$ are the chiral projector operators, $\tan \beta = v_u/v_d$ is the ratio of vaccum expectation values of the two Higgs doublets.

The trilinear couplings of Higgs bosons and W-boson are given by

$$\mathcal{L}_{(h^0, H^0, A^0)H^-W^+} = i \frac{g}{2} [\cos(\alpha - \beta) h^0 \overleftrightarrow{\partial}_\mu H^- + \sin(\alpha - \beta) H^0 \overleftrightarrow{\partial}_\mu H^- + i A^0 \overleftrightarrow{\partial}_\mu H^-] W^{+\mu} + h.c.$$

The squarks couplings to gluino, W-boson and Higgs are given by

$$\begin{aligned}\mathcal{L}_{\tilde{g}q\bar{q}} &= -\sqrt{2}T^a [\bar{q}(\mathbf{R}_{i1}^{\tilde{q}} P_R - \mathbf{R}_{i2}^{\tilde{q}} P_L) \tilde{g} \tilde{q}_i + \bar{\tilde{g}}(\mathbf{R}_{i1}^{\tilde{q}} P_R - \mathbf{R}_{i2}^{\tilde{q}} P_L) q \tilde{q}_i^*], \\ \mathcal{L}_{\tilde{t}^* \bar{b}W} &= i \frac{g}{\sqrt{2}} (\mathbf{R}_{i1}^{\tilde{b}} \mathbf{R}_{j1}^{\tilde{t}} W^{+\mu} \tilde{t}_j^* \overleftrightarrow{\partial}_\mu \tilde{b}_i + \mathbf{R}_{i1}^{\tilde{t}} \mathbf{R}_{j1}^{\tilde{b}} W^{-\mu} \tilde{b}_j^* \overleftrightarrow{\partial}_\mu \tilde{t}_i), \\ \mathcal{L}_{H^k \tilde{b}^* \tilde{b}} &= g G_{ij}^k H^k \tilde{b}_j^* \tilde{b}_i \quad (H^k = h^0, H^0, A^0), \\ \mathcal{L}_{H^k \tilde{t}^* \tilde{b}} &= \frac{g}{\sqrt{2}m_w} G_{ij}^k H^k \tilde{t}_j^* \tilde{b}_i + h.c. \quad (H^k = H^-),\end{aligned}$$

where

$$G_{ij}^k = [\mathbf{R}^{\tilde{b}} \hat{G}^k \mathbf{R}^{\tilde{b}T}]_{ij},$$

$$\hat{G}^{h^0} = \begin{pmatrix} -\frac{m_z}{\cos \theta_w} (\frac{1}{2} - \frac{1}{3} \sin^2 \theta_w) \sin(\alpha + \beta) + \frac{m_b^2}{2m_w \cos \beta} \sin \alpha & \frac{m_b}{2m_w \cos \beta} (A_b \sin \alpha + \mu \cos \alpha) \\ \frac{m_b}{2m_w \cos \beta} (A_b \sin \alpha + \mu \cos \alpha) & -\frac{1}{3} \frac{m_z}{\cos \theta_w} \sin^2 \theta_w \sin(\alpha + \beta) + \frac{m_b^2}{2m_w \cos \beta} \sin \alpha \end{pmatrix},$$

$$\hat{G}^{H^0} = \begin{pmatrix} \frac{m_z}{\cos \theta_w} (\frac{1}{2} - \frac{1}{3} \sin^2 \theta_w) \cos(\alpha + \beta) - \frac{m_b^2}{2m_w \cos \beta} \sin \alpha & -\frac{m_b}{2m_w \cos \beta} (A_b \cos \alpha - \mu \sin \alpha) \\ -\frac{m_b}{2m_w \cos \beta} (A_b \cos \alpha - \mu \sin \alpha) & \frac{1}{3} \frac{m_z}{\cos \theta_w} \sin^2 \theta_w \sin(\alpha + \beta) - \frac{m_b^2}{2m_w \cos \beta} \sin \alpha \end{pmatrix},$$

$$\hat{G}^{A^0} = \frac{im_b}{2m_w} \begin{pmatrix} 0 & -(A_b \tan \beta + \mu) \\ (A_b \tan \beta + \mu) & 0 \end{pmatrix},$$

$$\hat{G}^{H^-} = \begin{pmatrix} m_b^2 \tan \beta + m_t^2 \cot \beta - m_w^2 \sin 2\beta & m_b(A_b \tan \beta + \mu) \\ m_t(A_t \cot \beta + \mu) & \frac{2m_t m_b}{\sin 2\beta} \end{pmatrix},$$

where $R^{\tilde{q}}$ is a 2×2 matrix shown as below, which is defined to transform the squark current eigenstates to the mass eigenstates [21]:

$$\begin{pmatrix} \tilde{q}_1 \\ \tilde{q}_2 \end{pmatrix} = R^{\tilde{q}} \begin{pmatrix} \tilde{q}_L \\ \tilde{q}_R \end{pmatrix}, \quad R^{\tilde{q}} = \begin{pmatrix} \cos \theta_{\tilde{q}} & \sin \theta_{\tilde{q}} \\ -\sin \theta_{\tilde{q}} & \cos \theta_{\tilde{q}} \end{pmatrix},$$

with $0 \leq \theta_{\tilde{q}} < \pi$, by convention. Correspondingly, the mass eigenvalues $m_{\tilde{q}_1}$ and $m_{\tilde{q}_2}$ (with $m_{\tilde{q}_1} \leq m_{\tilde{q}_2}$) are given by

$$\begin{pmatrix} m_{\tilde{q}_1}^2 & 0 \\ 0 & m_{\tilde{q}_2}^2 \end{pmatrix} = R^{\tilde{q}} M_{\tilde{q}}^2 (R^{\tilde{q}})^\dagger, \quad M_{\tilde{q}}^2 = \begin{pmatrix} m_{\tilde{q}_L}^2 & a_q m_q \\ a_q m_q & m_{\tilde{q}_R}^2 \end{pmatrix},$$

with

$$\begin{aligned} m_{\tilde{q}_L}^2 &= M_{\tilde{Q}}^2 + m_q^2 + m_Z^2 \cos 2\beta (I_{3L}^q - e_q \sin^2 \theta_W), \\ m_{\tilde{q}_R}^2 &= M_{\tilde{D}}^2 + m_q^2 + m_Z^2 \cos 2\beta e_q \sin^2 \theta_W, \\ a_q &= A_q - \mu \tan \beta. \end{aligned}$$

Here, $M_{\tilde{q}}^2$ is the squark mass matrix. $M_{\tilde{Q}, \tilde{D}}$ and A_q are soft SUSY breaking parameters and μ is the higgsino mass parameter. I_{3L}^q and e_q are the third component of the weak isospin and the electric charge of the quark q , respectively.

Appendix B

In this Appendix, we will list the explicit expressions of the vertex, box and self-energy diagrams. For simplicity, we introduce the following abbreviations for the Passarino-Veltman two-point integrals B_i , tree-point integrals $C_{i(j)}$ and four-point integrals D_{ij} , which are defined similarly to Ref. [13] except that we take internal masses squared as arguments:

$$\begin{aligned} B_i &= B_i(t, m_{\tilde{g}}^2, m_{\tilde{t}_i}^2), \\ C_0^a &= C_0(0, s, 0, m_{\tilde{g}}^2, m_{\tilde{b}_i}^2, m_{\tilde{b}_j}^2), \\ C_i^b &= C_i(0, m_{H^-}^2, t, m_{\tilde{g}}^2, m_{\tilde{b}_i}^2, m_{\tilde{t}_j}^2), \\ C_{i(j)}^d &= C_{i(j)}(0, m_w^2, t, m_{\tilde{g}}^2, m_{\tilde{b}_i}^2, m_{\tilde{t}_j}^2), \\ D_{ij} &= D_{ij}(0, s, m_w^2, t, 0, m_{H^-}^2, m_{\tilde{g}}^2, m_{\tilde{b}_i}^2, m_{\tilde{b}_j}^2, m_{\tilde{t}_k}^2). \end{aligned}$$

The explicit expressions of the corresponding self-energy, vertex and box diagrams are given by

$$\begin{aligned}
\mathcal{M}^{vs} &= -\frac{2\alpha\alpha_s m_{\tilde{g}}}{\sin^2 \theta_w} \left[\frac{G_{ij}^{h^0} \cos(\alpha - \beta)}{s - m_{h^0}^2} + \frac{G_{ij}^{H^0} \sin(\alpha - \beta)}{s - m_{H^0}^2} + \frac{G_{ij}^{A^0}}{s - m_{A^0}^2} \right] [\tilde{R}_{i2} \tilde{R}_{j1} A_3 + \tilde{R}_{i1} \tilde{R}_{j2} A_4] C_0^a, \\
\mathcal{M}^{vt1} &= \frac{\alpha\alpha_s}{\sin^2 \theta_w m_w} \frac{G_{ij}^{H^-}}{t - m_t^2} \left[[\tilde{R}_{i1} \tilde{R}_{j1} t C_2^b + \tilde{R}_{i1} \tilde{R}_{j2} m_{\tilde{g}} m_t C_0^b] A_{10} \right. \\
&\quad \left. + [\tilde{R}_{i2} \tilde{R}_{j1} m_{\tilde{g}} C_0^b + \tilde{R}_{i2} \tilde{R}_{j2} m_t C_2^b] [A_{11} - 2A_3] \right], \\
\mathcal{M}^{vt2} &= \frac{2\alpha\alpha_s}{\sin^2 \theta_w m_w} \frac{\tilde{R}_{i1} \tilde{R}_{j1}}{t - m_t^2} \left[\tilde{R}_{i1} \tilde{R}_{j1} [m_t^2 \cot \beta [C_{00}^d A_{10} + C_{12}^d (A_6 - A_8)] + m_b \tan \beta [C_{00}^d (A_{11} - 2A_3) \right. \right. \\
&\quad \left. \left. + t C_{12}^d (A_3 - A_1)] \right] + \tilde{R}_{i1} \tilde{R}_{j2} m_{\tilde{g}} m_t C_1^d [\cot \beta (A_6 - A_8) + m_b \tan \beta (A_3 - A_1)] \right. \\
&\quad \left. - \tilde{R}_{i2} \tilde{R}_{j1} m_{\tilde{g}} C_1^d [m_t^2 \cot \beta (A_2 - A_4) + m_b \tan \beta (A_7 - A_5)] \right. \\
&\quad \left. + \tilde{R}_{i2} \tilde{R}_{j2} m_t [\cot \beta [C_{00}^d (A_{12} - 2A_4) + t C_{12}^d (A_4 - A_2)] \right. \\
&\quad \left. + m_b \tan \beta [C_{12}^d (A_5 - A_7) + C_{00}^d A_9] \right], \\
\mathcal{M}^{box} &= \frac{2\alpha\alpha_s}{\sin^2 \theta_w m_w} \tilde{R}_{j1} \tilde{R}_{k1} G_{ki}^{H^-} \left[\tilde{R}_{i1} \tilde{R}_{j1} [A_{10} D_{00} - A_6 (D_{13} + D_{23} + D_{33}) + A_8 (D_{23} + D_{33})] \right. \\
&\quad \left. + \tilde{R}_{i2} \tilde{R}_{j2} [A_9 D_{00} - A_5 (D_{13} + D_{23} + D_{33}) + A_7 (D_{23} + D_{33})] \right], \\
\mathcal{M}^{self} &= \frac{\alpha\alpha_s}{\sin^2 \theta_w} \frac{1}{(t - m_t^2)^2} \left[m_t \cot \beta [m_{\tilde{g}} (m_{H^-}^2 + m_t^2) \tilde{R}_{i1} \tilde{R}_{i2} B_0 + m_{H^-}^2 m_t B_1] A_{10} \right. \\
&\quad \left. + m_b \tan \beta [m_{H^-}^2 (\tilde{R}_{i1})^2 + 2m_{\tilde{g}} m_t \tilde{R}_{i1} \tilde{R}_{i2} B_0 + m_t^2 (\tilde{R}_{i2})^2 B_1] [A_{11} - 2A_3] \right],
\end{aligned}$$

where we omit the common color factor $T^a T^a$.

-
- [1] P. W. Higgs, Phys. Rev. Letter. 12 (1964) 132; Phys. Rev. 145 (1966) 1156; F. Englert and R. Brout, Phys. Rev. Lett. 13 (1964) 321; G. S. Guralnik, C. R. Hagen, and T. W. B. Kibble, Phys. Rev. Lett. 13 (1964) 585.
 - [2] H. P. Nilles, Phys. Rep. 110, 1 (1984); H. E. Haber and G. L. Kane, Phys. Rep. 117, 75 (1985); A. B. Lahanas and D. V. Nanopoulos, Phys. Rep. 145, 1 (1987); supersymmetry, edited by S. Ferrara (North Holland/World Scientific, Singapore, 1987), Vols. 1-2.
 - [3] Z. Kunszt and F. Zwirner, Nucl. Phys. B385, 3 (1992), and references cited therein.
 - [4] A. C. Bawa, C. S. Kim and A. D. Martin, Z. Phys. C 47, (1990) 75; L. G. Jin, C. S. Li,

- R. J. Oakes, and S. H. Zhu, Eur. phys. J. C 14,(2000) 91; S. H. Zhu, Phys. Rev. D 67, 075006 (2003); T. Plehn, Phys. Rev. D 67, 014018 (2003); E. L. Berger, T. Han, J. Jiang and T. Plehn, Phys. Rev. D 71, 115012 (2005).
- [5] S. Morreti and K. Odagiri, Phys. Rev. D 55, 5627 (1997).
- [6] E. Eichten et.al, Rev. Mod. Phys. 56 (1984) 579; N. G. Deshpande, X. Tata and D. A. Dicus, Phys. Rev. D 29, 157 (1984); A. Krause et al., Nucl. Phys. B 519 (1998) 85; A. A. Barrientos Bendezu and B. A. Kniehl, Nucl. Phys. B 568 (2000) 305; O. Brein and W. Hollik, Eur. Phys. J. C 13 (2000) 175.
- [7] D. A. Dicus, J. L. Hewett, C. Kao, T. G. Rizzo, Phys. Rev. D 40, 787 (1989).
- [8] A. A. Barrientos Bendezu and B. A. Kniehl, Phys. Rev. D 59, 015009 (1999); S. Moretti, K. Odagiri, Phys. Rev. D 59, 055008 (1999).
- [9] A. A. Barrientos Bendezu and B. A. Kniehl, Phys. Rev. D 63, 015009 (2001); O. Brein, W. Hollik and S. Kanemura, Phys. Rev. D 63, 095001 (2001).
- [10] Y. S. Yang, C. S. Li, L. G. Jin and S. H. Zhu, Phys. Rev. D 62, 095012 (2000).
- [11] W. Hollik, S. H. Zhu Phys. Rev. D 65, 075015 (2002).
- [12] A. Sirlin, Phys. Rev. D 22, 971 (1980); W. J. Marciano and A. Sirlin, Phys. Rev. D 22, 2695 (1980); 31, 213(E) (1985); A. Sirlin and W. J. Marciano. Nucl. Phys. B 189 (1981) 442; K. I. Aoki et al., Prog. Theor. Phys. Suppl. 73, (1982) 1.
- [13] A. Denner, Fortschr. Phys. 41, 307 (1993).
- [14] S. Eidelman et al. (Particle Data Group), Phys. Lett. B 592, 1 (2004).
- [15] S. G. Gorishny et al., Mod. Phys. Lett. A 5, 2703 (1990); Phys. Rev. D 43, 1633 (1991); A. Djouadi et al., Z. Phys. C 70, 427 (1996); Comput. Phys. Commun. 108, 56 (1998); M. Spira, Fortschr. Phys. 46, 203 (1998).
- [16] J. Pumplin et al., J. High Energy Phys. 07 (2002) 012.
- [17] M. Carena, D. Garcia, U. Nierste, and C. E. M. Wagner, Nucl. Phys. B 577, 88 (2000).
- [18] Damien M. Pierce, Jonathan A. Bagger, Ren Jie Zhang, Nucl. Phys. B 491, 3 (1997).
- [19] M. Drees and S. P. Martin, hep-ph/9504324.
- [20] A. Djouadi et al., hep-ph/0211331.
- [21] S. Kraml, hep-ph/9903257; J. Ellis and S. Rudaz, Phys. Lett. 128B, 248 (1983).

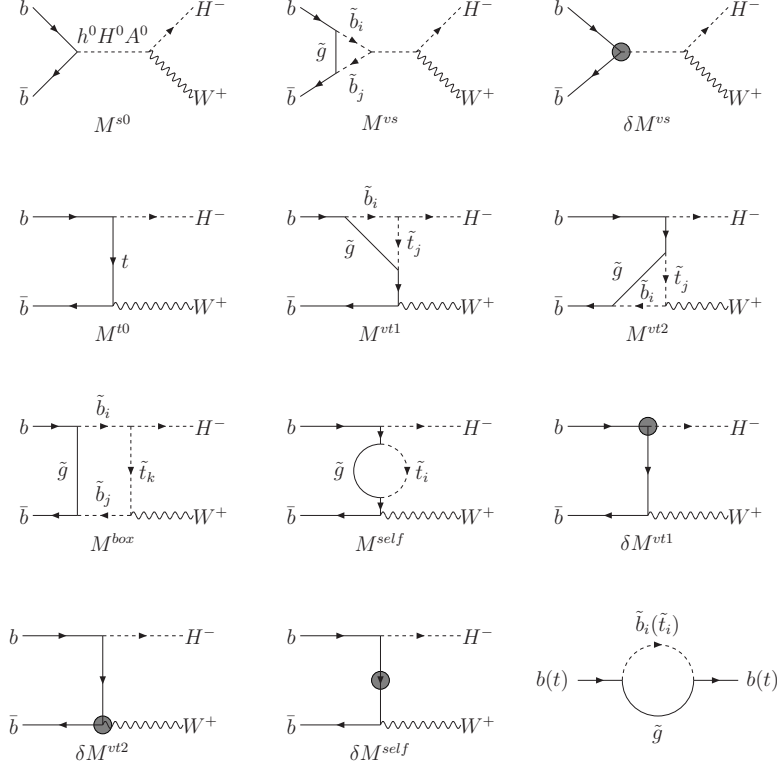


FIG. 1: Feynmann diagrams for the subprocess $b\bar{b} \rightarrow W^+ H^-$. Born diagrams: M^{s0}, M^{t0} ; Virtual correction diagrams: $M^{vs}, M^{vt1}, M^{vt2}, M^{box}, M^{self}$; Counter-term diagrams: $\delta M^{vs}, \delta M^{vt1}, \delta M^{vt2}, \delta M^{self}$.

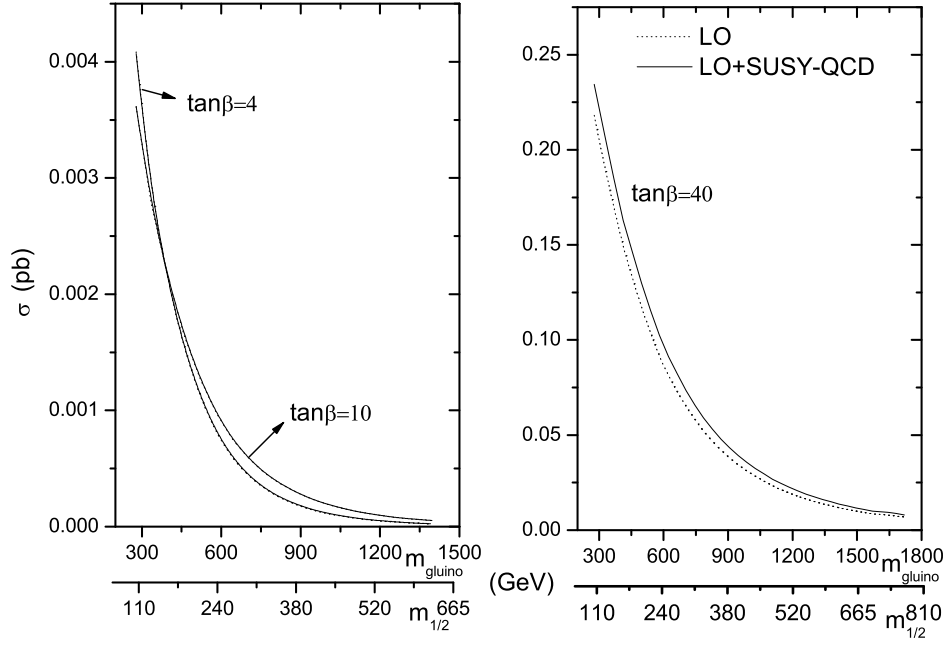


FIG. 2: Total cross sections for the W^+H^- production at the LHC as functions of m_{gluino} or $m_{1/2}$ for $\tan\beta = 4, 10$ and 40 , respectively, assuming: $m_0 = 200$ GeV, $A_0 = 250$ GeV, and $\mu < 0$.

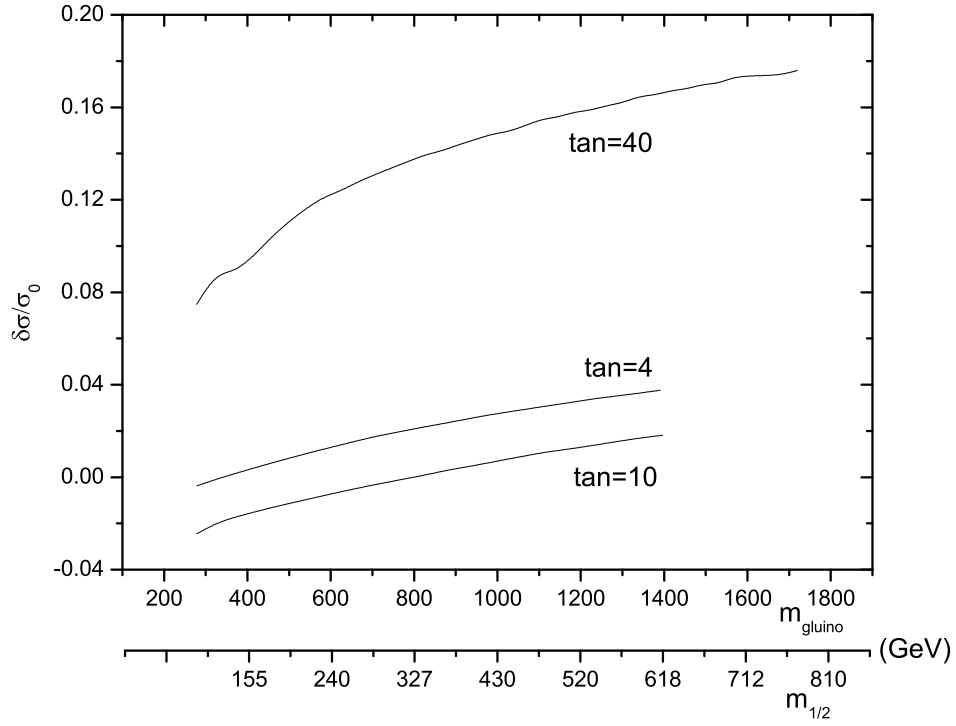


FIG. 3: The SUSY-QCD relative corrections to the cross sections for the W^+H^- production at the LHC as functions of m_{gluino} or $m_{1/2}$ for $\tan\beta = 4, 10$ and 40 , respectively, assuming: $m_0 = 200$ GeV, $A_0 = 250$ GeV, and $\mu < 0$.

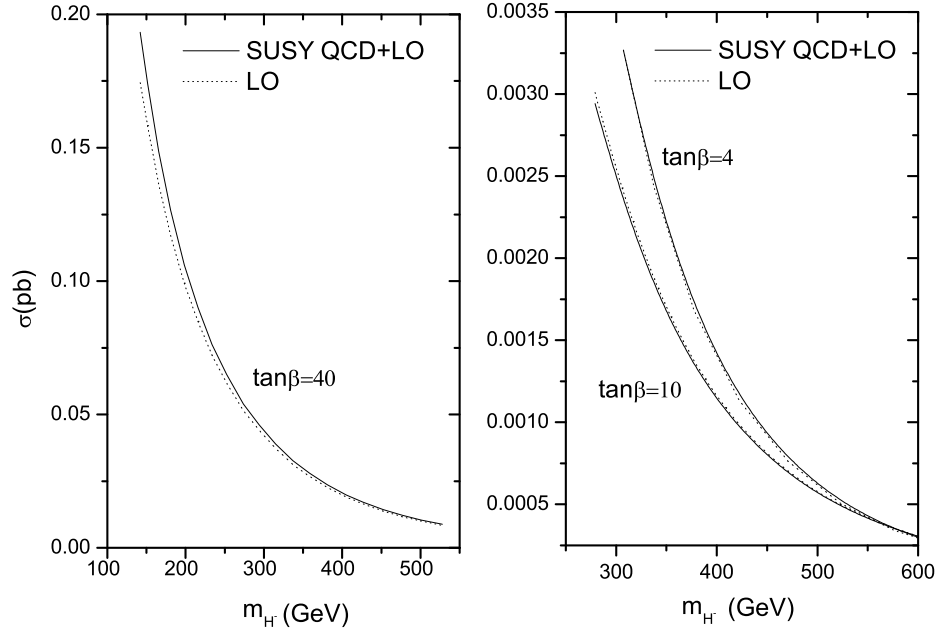


FIG. 4: Total cross sections for the W^+H^- production at the LHC as functions of m_{H^+} for $\tan\beta = 4, 10$ and 40 , respectively, assuming: $m_{1/2} = 180$ GeV, $A_0 = 250$ GeV., and $\mu < 0$.

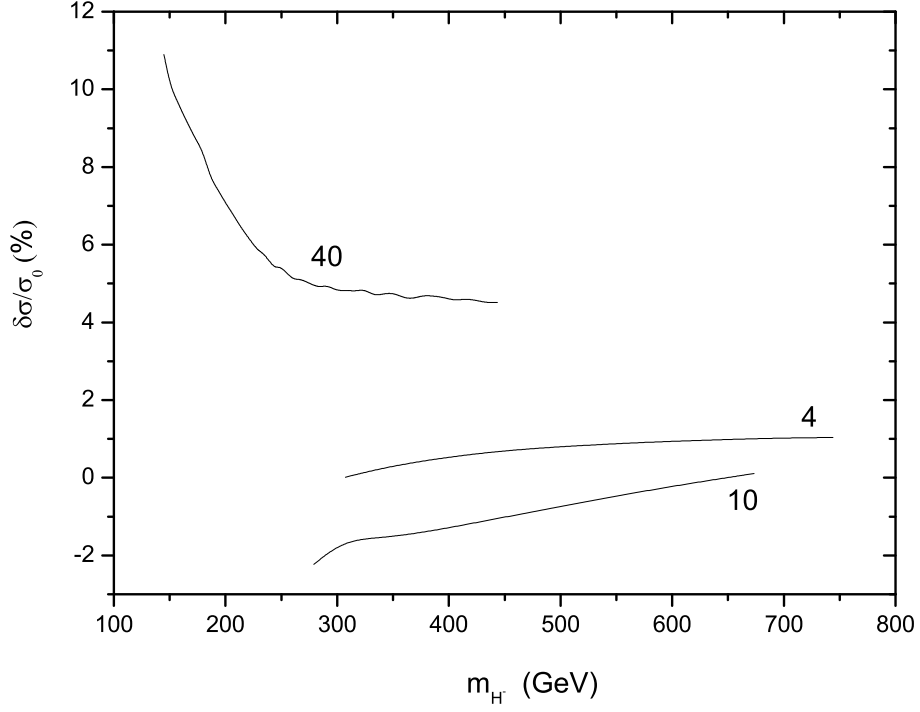


FIG. 5: The SUSY-QCD relative corrections to the cross sections for the W^+H^- production at the LHC as functions of m_{H^+} for $\tan\beta = 4, 10$ and 40 , respectively, assuming: $m_{1/2} = 180$ GeV, $A_0 = 250$ GeV., and $\mu < 0$.

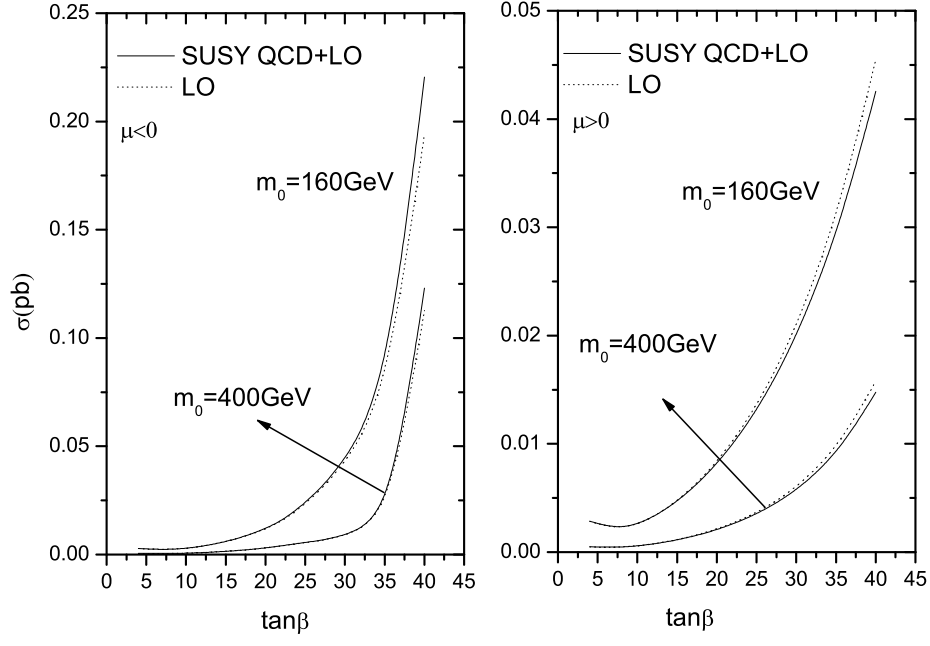


FIG. 6: Total cross sections for the W^+H^- production at the LHC as a function of $\tan\beta$ for $m_0 = 160$ GeV and 400 GeV, respectively, assuming: $A_0 = 300$ GeV, $m_{1/2} = 160$ GeV.

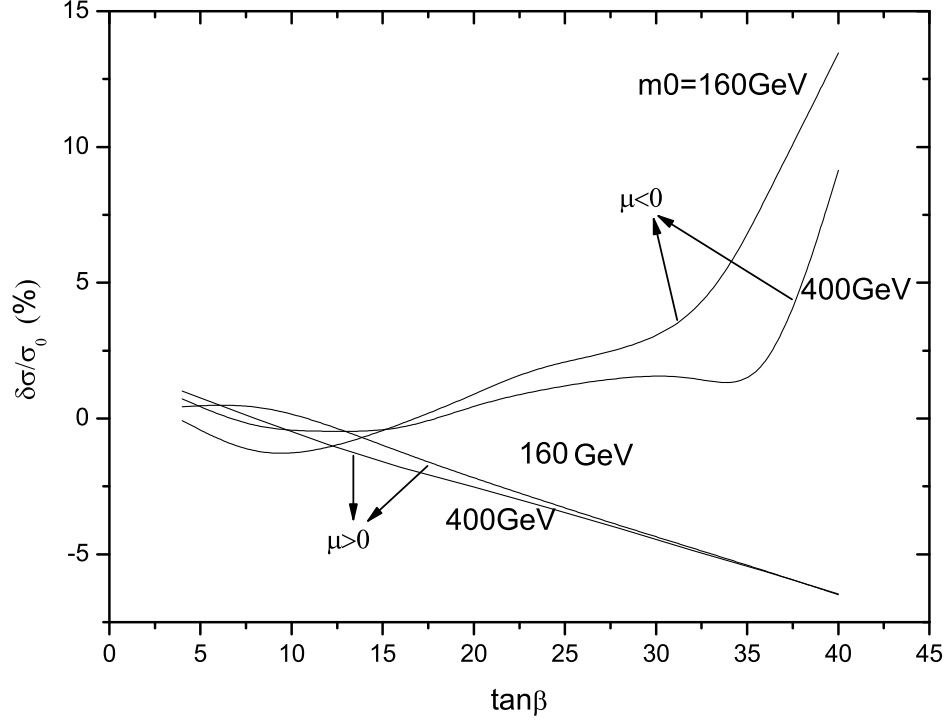


FIG. 7: The SUSY-QCD relative corrections to the cross sections for the W^+H^- production at the LHC as a function of $\tan\beta$ for $m_0 = 160$ GeV and 400 GeV, respectively, assuming: $A_0 = 300$ GeV, $m_{1/2} = 160$ GeV.

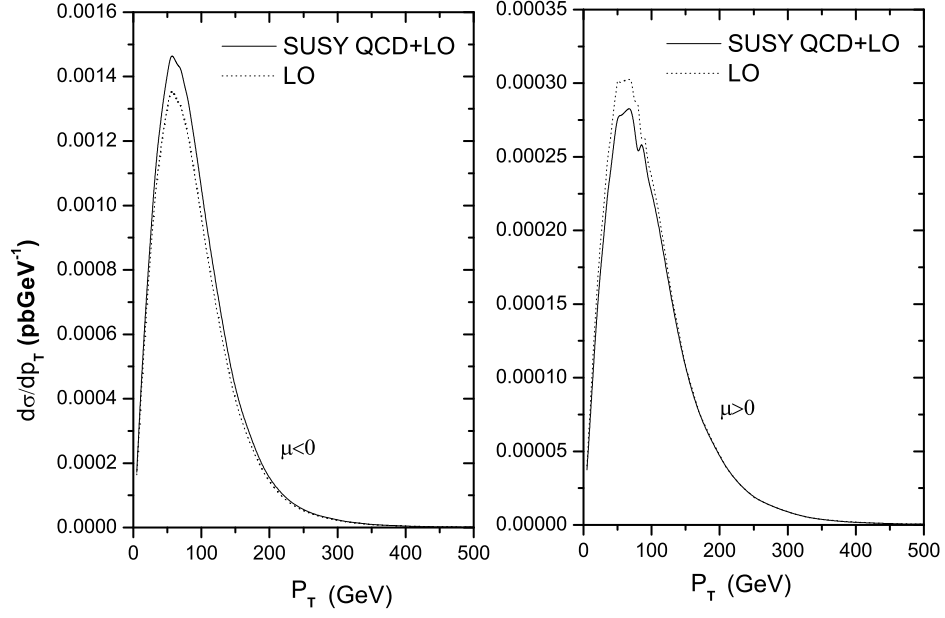


FIG. 8: Differential cross sections in the transverse momentum p_T of the W-boson for the W^+H^- production at the LHC, assuming: $m_0 = 200$ GeV, $m_{1/2} = 180$ GeV, $A_0 = 250$ GeV, and $\tan\beta = 40$.

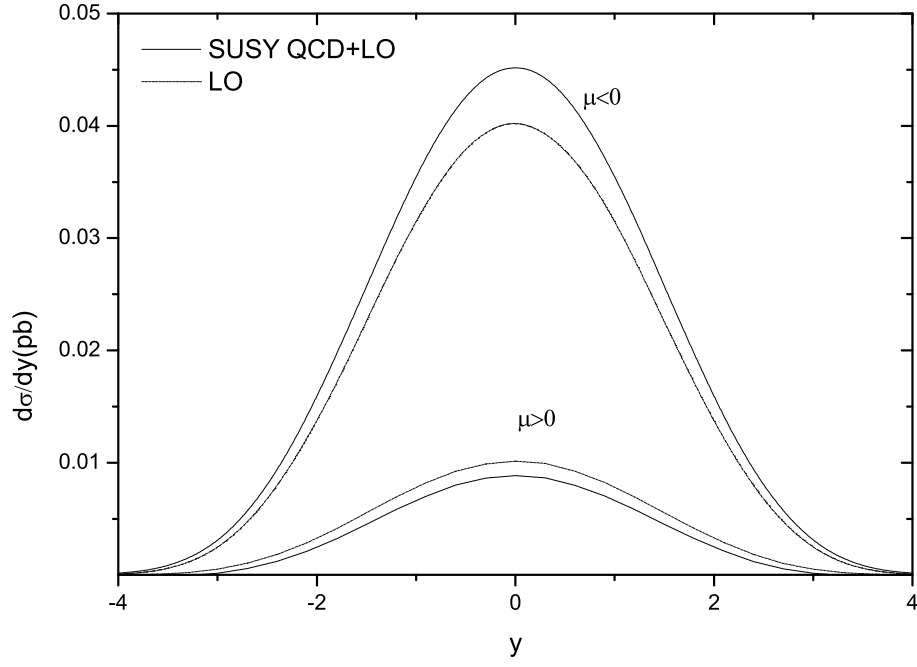


FIG. 9: Differential cross sections in the rapidity Y of the W -boson for the W^+H^- production at the LHC, assuming: $m_0 = 200$ GeV, $m_{1/2} = 180$ GeV, $A_0 = 250$ GeV, and $\tan \beta = 40$.

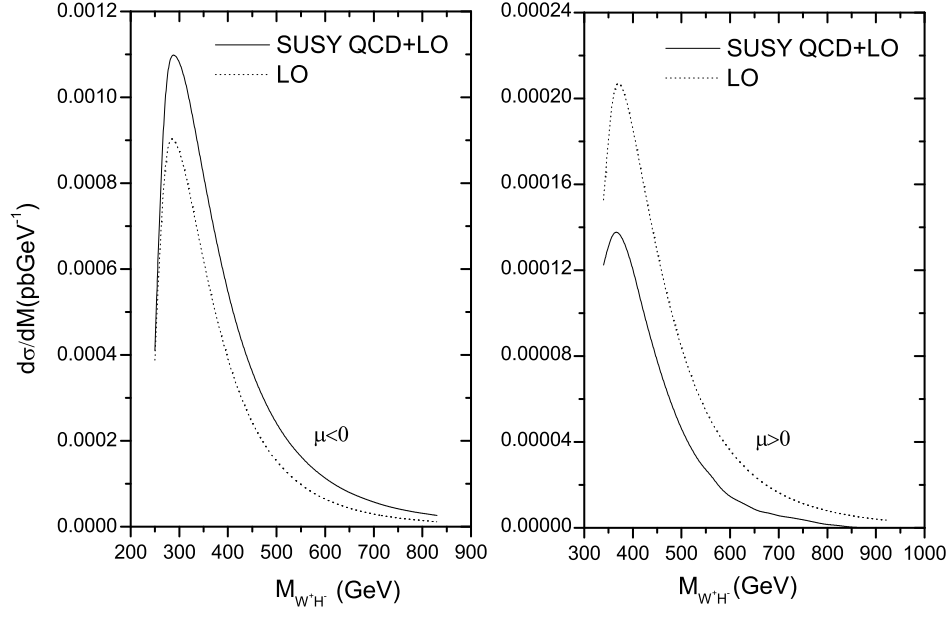


FIG. 10: Differential cross sections in the invariant mass for the W^+H^- production at the LHC, assuming: $m_0 = 200$ GeV, $m_{1/2} = 160$ GeV, $A_0 = 250$ GeV, and $\tan\beta = 40$.